Archives of Biochemistry and Biophysics 525 (2012) 53–59

Contents lists available at SciVerse ScienceDirect

Archives of Biochemistry and Biophysics

journal homepage: www.elsevier.com/locate/yabbi

The molecular details of WPD-loop movement differ in the protein-tyrosine phosphatases YopH and PTP1B ☆

Tiago A.S. Brandão [a,b], Sean J. Johnson [a,*], Alvan C. Hengge [a,*]

[a] Department of Chemistry and Biochemistry, Utah State University, Logan, UT 84322-0300, United States
[b] Departamento de Química, ICEX, Universidade Federal de Minas Gerais, Belo Horizonte, Minas Gerais 31270-901, Brazil

ARTICLE INFO

Article history:
Received 1 May 2012
and in revised form 3 June 2012
Available online 12 June 2012

Keywords:
Phosphatase
Protein-tyrosine phosphatase

ABSTRACT

The movement of a conserved protein loop (the WPD-loop) is important in catalysis by protein tyrosine phosphatases (PTPs). Using kinetics, isotope effects, and X-ray crystallography, the different effects arising from mutation of the conserved tryptophan in the WPD-loop were compared in two PTPs, the human PTP1B, and the bacterial YopH from *Yersinia*. Mutation of the conserved tryptophan in the WPD-loop to phenylalanine has a negligible effect on k_{cat} in PTP1B and full loop movement is maintained. In contrast, the corresponding mutation in YopH reduces k_{cat} by two orders of magnitude and the WPD loop locks in an intermediate position, disabling general acid catalysis. During loop movement the indole moiety of the WPD-loop tryptophan moves in opposite directions in the two enzymes. Comparisons of mammalian and bacterial PTPs reveal differences in the residues forming the hydrophobic pocket surrounding the conserved tryptophan. Thus, although WPD-loop movement is a conserved feature in PTPs, differences exist in the molecular details, and in the tolerance to mutation, in PTP1B compared to YopH. Despite high structural similarity of the active sites in both WPD-loop open and closed conformations, differences are identified in the molecular details associated with loop movement in PTPs from different organisms.

Introduction

Protein tyrosine phosphatases (PTPs)[1] comprise a large family of enzymes responsible for dephosphorylation of intracellular Tyr residues, functioning in concert with protein tyrosine kinases (PTKs) to modulate signal transduction pathways [1–4]. Two of the best-studied PTPs are the *Yersinia* protein tyrosine phosphatase, YopH, and the mammalian protein tyrosine phosphatase 1B (PTP1B). YopH is an essential virulence factor in the bacteria *Yersinia* sp., a genus that includes three species causative of human illness, ranging from gastrointestinal disease to Bubonic Plague [5]. YopH is also one of the most powerful phosphatases, catalyzing the hydrolysis of phosphate monoester dianions with k_{cat} values [6] of about 1300 s^{-1} for physiological phosphopeptide substrates at its pH optimum [7]. Comparison of this value with the rate constant for the uncatalyzed reaction of $\sim 10^{-20}$ s^{-1} ranks YopH as one of the most efficient enzymes known [8]. PTP1B is a biomedically important phosphatase with several activities, including negative regulation of insulin signaling by dephosphorylation of the insulin receptor tyrosine kinase [9]. As a result, this enzyme has been considered a significant target for treatment of type 2 diabetes and obesity [10,11]. PTP1B also down-regulates cell growth by dephosphorylating the epidermal growth factor receptor (EGFR) [12]. Overexpression has been observed in human breast and ovarian cancer, where it is believed to suppress potential tumors by antagonizing signaling of oncogenic factors [13,14]. Despite a similar active site and an identical mechanism, at its pH optimum PTP1B exhibits lower k_{cat} values of ~ 40 s^{-1} [15].

PTPs catalyze the hydrolysis of tyrosine phosphate esters by the two-step mechanism shown in Fig. 1 [2,3]. In the first step a nucleophilic cysteine thiolate attacks the substrate, resulting in formation of a phosphoenzyme intermediate with release of the peptidyl tyrosine. The second step involves attack of water on the phosphoenzyme intermediate and yields inorganic phosphate and the free enzyme. The central binding site for the phosphoryl group of the substrate is the P-loop, a signature motif region with the sequence CX_5R that includes the nucleophilic cysteine, a highly conserved arginine residue, and backbone amide groups oriented in a semicircular fashion. This arrangement provides hydrogen bonding to the phosphoryl group of the substrate and transition state (TS) stabilization.

Substrate binding in PTPs favors the closure of a flexible loop bearing the conserved sequence WPD. The aspartic acid in this loop functions as a general acid in the first step and as a general base

☆ This work was supported by National Institutes of Health Grant GM47297 (A.C.H.).
* Corresponding authors. Fax: +1 435 797 3390.
E-mail addresses: sean.johnson@usu.edu (S.J. Johnson), alvan.hengge@usu.edu (A.C. Hengge).
[1] *Abbreviations used:* PTPs, protein tyrosine phosphatases; PTKs, protein tyrosine kinases; PTP1B, protein tyrosine phosphatase 1B; EGFR, epidermal growth factor receptor; TS, transition state; KIEs, kinetic isotope effects.

0003-9861/$ - see front matter © 2012 Elsevier Inc. All rights reserved.
http://dx.doi.org/10.1016/j.abb.2012.06.002

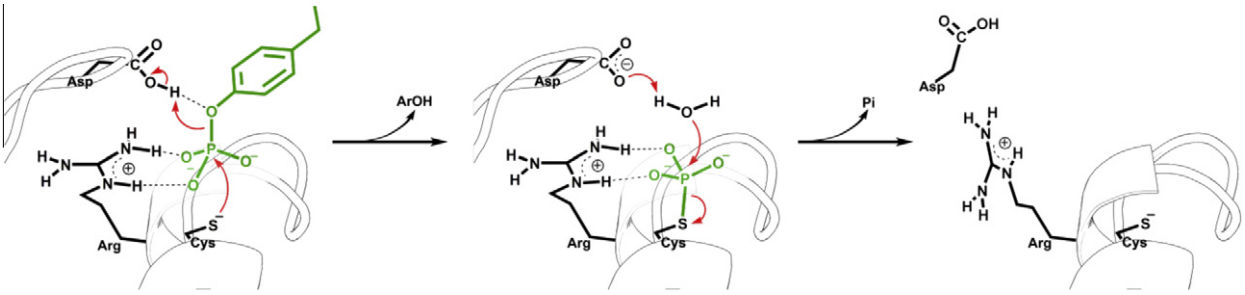

Fig. 1. The general mechanism of the PTP-catalyzed reaction. The WPD-loop assumes a catalytically active closed conformation with the general acid in position to protonate the leaving group during formation of the phosphoenzyme intermediate. In the second step this intermediate is hydrolyzed. After the phosphate product is released the WPD-loop open conformation becomes favored.

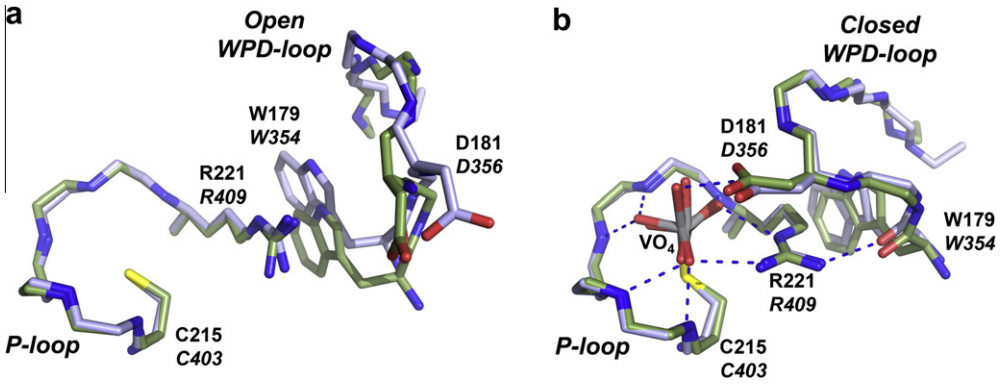

Fig. 2. Orientation of key residues at the active site of PTP1B (light blue) and YopH (green). (a) Superimposition of the ligand-free structures with the WPD-loop in the open conformation. (b) Superimposition of the vanadate-bound structures with WPD-loop in the closed conformation, using the same orientation as in (a). The lower, italicized residue positions refer to YopH. For the sake of clarity the only backbone carbonyl group is that of W179/W354 shown in (b). Hydrogen bonds in dotted blue lines are shown only for PTP1B. The PDB IDs used to generate each structure were: PTP1B wildtype: 2CM2 (ligand-free form, open WPD-loop) [42] and 3I80 (VO_4 bound, closed WPD-loop) [28]; YopH wildtype: 1YPT (ligand-free form, open WPD-loop) [19] and 2I42 (VO_4 bound, closed WPD-loop). (For interpretation of the references to colour in this figure legend, the reader is referred to the web version of this article.)

catalyst in the second step (Fig. 1) [16,17]. The WPD-loop has two distinct conformations, an "open" conformation in which the WPD-loop has negligible interaction with the P-loop; and a "closed" conformation, where the WPD-loop is folded over the active site, bringing the conserved Asp residue up to 8 Å closer to the bound substrate [18–22]. The loop-open and closed forms of the active sites of YopH and PTP1B superimpose well with one another (Fig. 2). The backbone residues of the P-loop align closely in both the ligand-free and ligand-bound states. Unlike the WPD loop, there is no evidence for significant motion of the P-loop during catalysis.

Mechanistic investigations have shown that the overall mechanism and the transition state for the chemical steps are the same for these two PTPs, as they are for all PTPs that have been examined [23]. Despite the structural and mechanistic similarities, the catalytic rates of YopH and PTP1B vary by more than an order of magnitude, and rates vary even more within other members of the PTP family. This has led us to inquire whether there are differences in the molecular details involved in loop movement between PTPs. Thus, we have compared the effect of the Trp mutation in PTP1B and YopH. This highly conserved residue is not directly involved in catalysis, but is involved in WPD loop motion. During loop movement the indole side chain slides within a hydrophobic crevice. Kinetic data and isotope effects on the reaction with the substrate *p*NPP were obtained, and crystal structures for ligand-free and bound states of Trp to Phe mutant of PTP1B are reported. Analogous kinetic and structural data for the corresponding mutant of YopH have previously been reported [17,24,25], which allows for direct comparisons with data obtained with PTP1B. Unexpectedly, the conservative Trp to Phe mutation has significantly different effects in the two enzymes.

Materials and methods

The plasmid pEt-19b encoding the 37 kDa form of the human wildtype PTP1B (amino acid residues 1–321) was provided by Dr. Nicholas K. Tonks and has been previously reported [26]. Labeled and natural abundance *p*-nitrophenyl phosphate (*p*NPP, dicyclohexylammonium salt) were synthesized according to previous methods [27]. Sodium orthovanadate (Na_3VO_4) was purchased from Fisher Scientific©.

Site-directed mutagenesis

Mutations in PTP1B were made by using the QuikChange® site-directed mutagenesis kit from Strategene©. The oligonucleotide primers used to insert the desired mutations were as follows: W179F, ccactataccacattccctgactttggagtccctg; and W179A, ccactataccacagccgcctgactttggagtccctg. The underlined bases refer to the changes from the naturally occurring nucleotides. All mutations were verified by DNA sequencing.

Protein expression and purification

PTP1B mutants were expressed in *Escherichia coli* and purified to homogeneity as previously reported for the wild-type protein [28]. All Trp mutations were verified by TOF–MS. Protein

concentrations were monitored by UV using an $A_{1mg/mL}^{280nm}$ = 1.10 for both tryptophan PTP1B mutants.

Kinetics

Reactions were carried out at 23 °C using the substrate *p*NPP in the presence of 1 mM DTT in a three-component buffer mixture of 100 mM sodium acetate, 50 mM Bis–Tris, and 50 mM Tris, which provides a constant ionic strength over a wide pH range. Reactions were initiated by addition of enzyme (final reaction volume of 300 μL) and quenched by addition of 30 μL of 10 M NaOH. The non-enzymatic hydrolysis of the substrate was corrected by measuring the respective reaction in the absence of enzyme. The initial rate measurements for the enzyme catalyzed hydrolysis of *p*NPP were monitored by product (*p*-nitrophenol) formation, which was measured from the absorbance at 400 nm using a molar extinction coefficient of 18,300 M^{-1} cm^{-1}. Kinetic parameters were determined by a fit of the initial rate (v) versus [*p*NPP] data to the Michaelis–Menten equation.

Inhibition constants (K_i) for PTP1B by tungstate and molybdate for the W179F mutant of PTP1B were determined by measuring initial rates of *p*NPP hydrolysis as described above in the presence of a range of concentrations of inhibitor (0–10 K_i) and [*p*NPP] (0.5–6 K_m) at pH 5.5 and 23 °C. Inhibition constants were obtained from a global fit, considering that $K_m^{ap} = K_m(1 + [I]/K_i)$ in the presence of inhibitors. The V_{max} values were unchanged in the presence of these inhibitors, as expected for competitive behavior.

Kinetic isotope effect determinations

Kinetic isotope effects (KIEs) were measured using the internal competition method, and thus are isotope effects on V/K [29]. In the commonly used notation, a leading superscript of the heavier isotope is used to indicate the isotope effect on the following kinetic quantity; for example $^{15}(V/K)$ denotes $(V/K)_{14}/(V/K)_{15}$, the nitrogen-15 KIE on V/K.

Natural abundance *p*NPP was used for measurements of $^{15}(V/K)$. The ^{18}O KIEs $^{18}(V/K)_{bridge}$ and $^{18}(V/K)_{nonbridge}$ were measured by the remote label method, using the nitrogen atom in *p*-nitrophenol as a reporter for isotopic fractionation in the labeled oxygen positions [23]. The isotopic isomers used are shown in Supporting information. Isotope effect determinations were made at 25 °C in 50 mM Bis–Tris buffer, pH 5.5, containing 1 mM DTT. The *p*NPP concentration was 18 mM and the reactions were started by addition of PTP1B wild-type or mutant to a final concentration of 0.15 μM. After reactions reached 40–60% completion (about 1 h.) they were stopped by titrating to pH 3–4 with HCl. Protocols for isolation of *p*-nitrophenol, isotopic analysis and calculation of the isotope effects were the same as previously described [30], and are described in Supporting information.

Crystallization

Crystals were grown using sitting drop vapor diffusion at 4 °C. The crystallization drop was prepared by mixing 2 μL of protein solution, 0.5 μL sucrose 30% (w/v) and 3 μL of precipitant solution (0.1 M Hepes pH 7.5, 0.2 M magnesium acetate and 15–20% polyethylene glycol 8000). The well solution was 500 μL of precipitant solution. The protein solution used to obtain the ligand-free crystal was 12 mg/mL PTP1B W179F in 10 mM Tris pH 7.5, 25 mM NaCl, 0.2 mM EDTA and 3 mM DTT; the vanadate bound crystals were grown using 15 μL of 12 mg/mL PTP1B W179F and 0.5 μL of 60 mM of Na_3VO_4 (1–4.7 eq. mol protein–vanadate ratio). Single crystals were visible after three days. Cryoprotection was performed by transferring crystals stepwise into stabilization solution with increasing glycerol amounts to a final concentration of 15% and the respective initial concentrations of ligands present in the protein and precipitant solutions, and then flash-cooled in liquid nitrogen.

Data collection, structure determination and refinement

Diffraction data were collected on a home source (Rigaku Raxis IV++). Data for the PTP1B W179F ligand-free structure was indexed and processed using DENZO and SCALEPACK in the HKL2000 program suite [31] and PTP1B W179F bound with vanadate was using d*TREK in the program Crystal Clear [32]. Molecular replacement was performed using Phaser [33] from the CCP4 program suite [34,35]. The search model was the ligand-free wildtype PTP1B structure (PDB ID 2CM2) with the active site water molecules removed. Refinement was performed using the program Phenix [36]. Coot [37] and MolProbity [38] were used for model building and validation. Structure factors were deposited in the Protein Data Bank. Table 1 summarizes the crystallographic data, statistics of structure refinement and PDB accession numbers. All figures depicting crystallography data were prepared using Pymol [39].

Table 1
Data collection and refinement statistics for structures of PTP1B W179F ligand-free and vanadate bound. Values in parentheses correspond to those in the outer resolution shell.

	PTP1B W179F ligand-free	PTP1B W179F VO_4
Data collection		
Beamline	Home source	Home source
Wavelength (Å)	1.5418	1.5418
Resolution range (Å)	38.23–2.05	38.37–2.20
Outer shell (Å)	2.12–2.05	2.28–2.20
No. of reflections		
Unique	29,808	24,220
Total	174,588	133,515
Average redundancy	5.9 (6.1)	5.5 (5.6)
Mean $I/(I)$	15.1 (2.7)	7.9 (2.7)
Completeness (%)	98.7 (97.8)	98.7 (97.3)
R_{sym} (%)[a]	10.3 (64.9)	10.8 (49.4)
Space group	$P3_121$	$P3_121$
Number of protein molecules per asymmetric unit	1	1
Unit cell dimensions		
a, b, c (Å)	88.3, 88.3, 104.5	88.6, 88.6, 104.3
α, β, γ (°)	90.0, 90.0, 120.0	90.0, 90.0, 120.0
Refinement		
R_{work}/R_{free} (%)[b]	20.4/24.5	19.6/25.4
Atoms in the structure		
Protein	2372	2485
Waters	239	276
Ligands/ions	20	31
Average B factors (Å^2)		
Protein	38.19	41.97
Water	45.48	49.81
Ligands/ions	61.79	66.04
Rmsd bond (Å)/angle (°)	0.008/1.104	0.009/1.172
Protein geometry [c]		
Ramachandran outliers (%)	0.35	0.34
Ramachandran favored (%)	97.6	98.0
Rotamer outliers (%)	0.76	0.37
PDB ID	3QKP	3QKQ

[a] $R_{sym} = (\Sigma|(I-\langle I\rangle)|)/(\Sigma I)$, where $\langle I\rangle$ is the average intensity of multiple measurements.

[b] $R_{work} = (\Sigma||F_{obs}|-|F_{calc}||)/(\Sigma|F_{obs}|)$ and is calculated using all data; R_{free} is the R-factor based on 5% of the data excluded from refinement.

[c] Ramachandran statistics were calculated using the MolProbity server [38].

Results

Kinetic properties of the PTP1B W179F and W179A mutants

Table 2 shows the kinetic data at several pH values, near the reported pH optimum for PTP1B, for hydrolysis of *p*NPP catalyzed by PTP1B wildtype and W179 mutants. For comparison, in the lower section of Table 2 are presented the previously reported kinetic data for wildtype YopH and its corresponding tryptophan mutants.

The native enzymes exhibit bell shaped pH-profiles for k_{cat} with pH optima close to 5.5 [15,25]. The acidic limb results from deprotonation of the cysteine residue to produce the active thiolate nucleophile (Cys215 in PTP1B). On the basic limb, enzymatic activity is reduced at high pH due to loss of general acid catalysis by the aspartic acid residue (Asp181 in PTP1B). Our interest is focused on the retention or loss of general acid catalysis by mutation of the tryptophan in the WPD loop of PTP1B to Phe and Ala. The loss of general acid catalysis should reduce k_{cat} by orders of magnitude even with the activated substrate *p*NPP; moreover, k_{cat} values would not decrease above the pH optimum due to the change from bell to a half-bell pH dependency. In contrast, if general acid catalysis is retained, a much smaller effect on k_{cat} should be observed at the optimum pH, and a monotonic decrease in this value above the optimum would be expected due to the incorrect protonation state of the general acid.

The k_{cat} value for the W179F mutant at pH 5.5 is decreased only ~2-fold in relation to the wildtype enzyme, and k_{cat} decreases as pH increases (Table 2). This differs from the effect of the corresponding mutation in YopH. The k_{cat} values for YopH W354F are very similar from pH 5.5 to 7.5, ranging from 3 to 1 s^{-1}, and are about 200-fold lower at pH 5.5 than for the wildtype enzyme.

The activity of PTP1B is more strongly affected by the W179A mutation, and mirrors the effect of the corresponding mutation in YopH (Table 2). When compared to the k_{cat} values at pH 5.5 for the native enzymes, the k_{cat} values in PTP1B W179A and YopH W354A are approximately 320- and 480-fold lower, respectively. In each case, k_{cat} values are also similar in the pH range of 5.5 and 7.5, which indicates that general acid catalysis is strongly impaired by this mutation.

Table 3 shows the effect of tungstate and molybdate on the hydrolysis of *p*NPP catalyzed by PTP1B wildtype and the W179F mutant. For comparison purposes the lower section of this table displays reported inhibition data for tungstate for YopH wildtype and W354F mutant. The activity of PTP1B wildtype and W179F are inhibited by similar extents in both cases, with inhibition constants in the micromolar range for both competitive inhibitors. On the other hand, YopH W354F exhibits reduced affinity (about 5-fold) toward tungstate compared to the wildtype [25]. This reduced affinity has been attributed to an improper structure alignment for oxyanion binding, which is not observed by the corresponding W179F mutation in PTP1B.

Table 3
Inhibition constants by oxyanions for wildtype and tryptophan mutants of PTP1B[a] and YopH[b]. All measurements were made at 25 °C using *p*NPP as substrate.

Reaction	K_i (μM) for tungstate	K_i (μM) for molybdate
PTP1B wildtype	0.99(7)	0.17(2)
PTP1B W179F	0.62(4)	0.26(4)
YopH wildtype	5.8	
YopH W354F	32.0	

[a] Values in parenthesis are the standard deviations in the last decimal place.
[b] Data from Keng et al. [25] measured at pH 5.5.

Kinetic isotope effects

The KIEs for the hydrolysis of *p*NPP by wildtype PTP1B have been previously reported [28]. These and the KIE data for the PTP1B mutants obtained in this work are shown in Table 4. Because the enzymatic substrate of PTPs is the dianionic form, the $^{18}(V/K)_{nonbridge}$ isotope effect was corrected for the isotope fractionation for protonation of the nonbridge oxygen atoms, as *p*NPP is present as a mixture of monoanion and dianion forms under the conditions of the experiment. The KIE data in the leaving group for the W179F mutant are similar to those for the wildtype PTP1B, with a negligible $^{15}(V/K)$ KIE and a primary bridge-$^{18}(V/K)$ KIE ranging from 1.2% to 1.4%. For comparison, previously reported KIEs for wildtype YopH [30] and for YopH mutant [27] corresponding to the Trp to Phe mutation in PTP1B that were examined in this study are shown in the lower section of Table 4.

The expected ranges of the isotope effects in *p*NPP and their interpretation have been discussed in detail previously [23,40], and are summarized briefly here. The KIE at the nitro nitrogen atom, $^{15}(V/K)$, arises from negative charge development on the nitrophenolate leaving group. When general acid catalysis maintains the leaving group in a neutral state there is no isotope effect (KIE = unity), while in general acid mutants of PTPs $^{15}(V/K)$ reaches its maximum value of about 1.003, reflecting a full negative charge. The KIE at the bridge oxygen atom, $^{18}(V/K)_{bridge}$, arises from P–O bond fission and is also affected by O–H bond formation by the general acid. Bond fission produces normal isotope effects, while bond formation gives rise to inverse effects. The normal effect from P–O fission is large, and in general acid mutants of PTPs the $^{18}(V/K)_{bridge}$ effect is near its maximum of 1.03 reflecting a largely broken P–O bond in the transition state. In native enzymes where general acid catalysis takes place, the observed $^{18}(V/K)_{bridge}$ is reduced by protonation, as shown in Table 4.

The $^{15}(V/K)$ and $^{18}(V/K)_{bridge}$ KIEs are the reporters for how general acid catalysis might be compromised by mutation. Loss of general acid will result in an increase in both of these isotope effects relative to their values in the native enzymes. The isotope effect in the nonbridging oxygen atoms, $^{18}(V/K)_{nonbridge}$, monitors the hybridization state of the transferring phosphoryl group. A loose

Table 2
Top, kinetic constants at different pHs for *p*NPP hydrolysis catalyzed by the wildtype PTP1B and tryptophan 179 mutants at 23 °C.[a] Below, kinetic constants for the reaction of *p*NPP by the wildtype and YopH variants with mutations to the corresponding residue. [b]

Reaction	K_m (mM) at pHs			k_{cat} (s^{-1}) at pHs		
	5.5	6.5	7.5	5.5	6.5	7.5
PTP1B wildtype	0.58(2)	1.48(2)	2.20(1)	24.4(2)	17.1(1)	3.48(1)
PTP1B W179F	0.93(5)	0.86(3)	1.04(5)	11.8(2)	2.42(2)	0.151(3)
PTP1B W179A	4.41(9)	3.94(3)	2.85(5)	0.0750(5)	0.0667(1)	0.0370(2)
YopH wildtype	2.00			601	95.5	11.0
YopH W354F	4.82			2.96	1.42	1.10
YopH W354A	3.85			1.26	1.23	1.07

[a] Values in parenthesis are the standard deviations in the last decimal place.
[b] YopH data were taken from Keng et al. [25] and were measured at 30 °C.

Table 4
Top, isotope effects for catalyzed reaction of *p*NPP by the wildtype and W179F mutant of PTP1B. Below, isotope effects for the reaction of *p*NPP by the wildtype and YopH Trp mutation corresponding to that in PTP1B.[a]

Reaction	$^{15}(V/K)$	$^{18}(V/K)_{bridge}$	$^{18}(V/K)_{nonbridge}$	Reference
PTP1B wildtype[b]	1.0004(2)	1.0121(9)	1.0018(5)	[28]
PTP1B W179F[b]	1.0006(1)	1.0140(9)	1.0021(7)	This work
YopH wildtype[c]	0.9999(3)	1.0152(6)	0.9998(13)	[30]
YopH W354F[c]	1.0013(2)	1.0240(10)	1.0015(8)	[27]

[a] Values in parenthesis are the standard errors in the last decimal place.
[b] pH 5.5 and 25 °C.
[c] pH 5.5 and 30 °C.

or metaphosphate-like transition state gives rise to slightly inverse effects. This isotope effect becomes increasingly normal as the transition state grows more associative in nature.

Crystallography

We have solved X-ray structures for PTP1B W179F in the presence and absence of the competitive inhibitor vanadate. Fig. 3 shows the active site of PTP1B W179F. In the crystal grown in the presence of vanadate, two conformations are observed at approximately equal occupancy: a WPD loop-open ligand-free form, and a closed vanadate-bound form (refined to 48% and 52% occupancy, respectively). A difference density map for vanadate is shown in Fig. S3 of Supporting information. Conformational differences between these two forms are confined to the side chain of Arg221 and the WPD-loop. The open form observed at 48% occupancy in the crystal grown in the presence of vanadate is superimposable with both the ligand-free structure of W179F, as well as the wildtype PTP1B (PDB ID 2CM2) (see Supporting information Fig. S2). In the closed form, the bound vanadate exhibits a trigonal bipyramidal conformation with apical positions occupied by the Cys215 sulfur and an oxygen atom from a water molecule. The three equatorial oxygen atoms hydrogen bond to main chain NH amides in the P-loop and to the guanidinium moiety of Arg221. Compared to the open form, the side chain of Arg221 is rotated about 100° around chi-3 and hydrogen bonds to the carbonyl group of Phe179. The side chain of Phe179 is embedded into a hydrophobic pocket in both the open and closed forms, with the Phe methylene groups of these two forms ~1.4 Å apart. Similarly, the respective distance between the Trp methylene groups in the open and closed forms of the wildtype enzyme is ~1.2 Å, and the

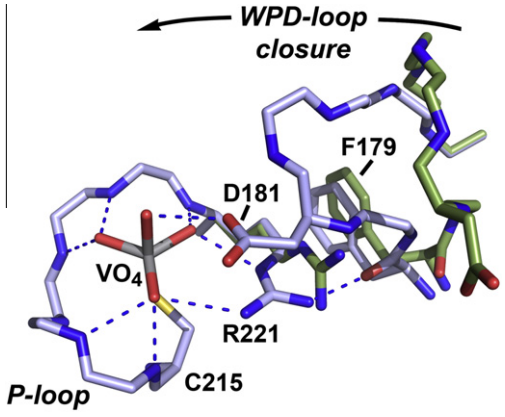

Fig. 3. Orientation of key residues at the active-site of PTP1B W179F in unbound, loop-open (green) and vanadate-bound, loop-closed (light blue) states. (For interpretation of the references to colour in this figure legend, the reader is referred to the web version of this article.)

Phe and Trp rings are similar in their positions and orientations. Other residues at the bottom of the Trp/Phe pocket (*i.e.* Phe191 and Phe 269) and at the WPD-loop region of PTP1B wildtype and W179F mutant also exhibit similar conformational changes from the open to the closed forms. As a whole, the structure of PTP1B W179F with vanadate bound represents a transition state analog of the second catalytic step, showing structural characteristics similar to those of a vanadate complex of the wildtype enzyme [28].

Discussion

Fig. 2 shows an overlay of the open and closed conformations in the active sites of the YopH and PTP1B wild-type enzymes. Upon oxyanion or substrate binding to the P-loop, the conserved Arg residue rotates to make two hydrogen bonds with the oxyanion. In addition, a new hydrogen bond formed between the guanidinium group of Arg and the carbonyl oxygen atom of the conserved Trp assists in stabilizing the WPD loop in the closed, catalytically active position. All PTPs share these essential aspects of binding and catalysis. In the following discussion we present our findings as revealed by kinetics, structural analysis, and isotope effects of the distinctive effect of Trp mutations in the catalysis of these two enzymes.

The Trp residue (W179 in PTP1B and W354 in YopH) is highly conserved in the PTP family and forms one of the so-called hinge residues of the flexible loop. In the superposition of the ligand-free, loop-open structures of the two enzymes, the respective indole rings and backbones are adjacent to one another (~2 Å apart) and the residues adopt very similar positions in the respective loop-closed structures (see Fig. 2 for an overlap of these structures).

A previous study revealed that the conservative W354F mutation in YopH results in a decrease in k_{cat} by two orders of magnitude, loss of the basic limb of the pH-rate profile, and kinetic isotope effects indicative of the leaving group departing as an anion [25,27]. These data indicate the loss of general acid catalysis in the mutant. Subsequent structural analyses in the presence and absence of bound ligands showed that the WPD loop is fixed in a quasi-open position by the W354F mutation, leaving the Asp 356 side chain in a position unproductive for catalysis [24].

In contrast, the corresponding W179F mutant of PTP1B has minor effects on k_{cat} (about 2-fold decrease at pH 5.5) compared to wild-type (Table 2). The KIE data are similar to those of the wildtype enzyme (Table 4), showing that general acid catalysis remains effective. The ability of PTP1B to bind the competitive inhibitors tungstate and molybdate is also not affected by the W179F mutation (Table 3). In contrast, the corresponding mutation in YopH reduces the binding affinity for tungstate by about 6-fold at pH 5.5 [25].

The crystal structure of the W179F mutant of PTP1B shows both loop open and closed forms, in contrast to structures of W354F YopH. This clearly demonstrates the ability of the WPD loop in W179F PTP1B to attain both the open and fully closed conformations. In light of the unexpected difference in the effect of this mutation in the two enzymes, we closely examined these structures looking for differences that might explain the retention of full loop movement in PTP1B W179F, while the loop of the corresponding YopH W354F mutant locks in an unproductive position. In both wildtype enzymes the indole ring of Trp is embedded in a hydrophobic pocket and undergoes a repositioning upon loop closure. Interestingly, a comparison of the loop open and closed crystal structures reveals a difference in the movement of the Trp side chains (Fig. 4). In the PTP1B wildtype and W179F mutant, the Trp/Phe side chains slide in the same direction as WPD-loop movement. The Phe side chain in the W179F mutant encounters no

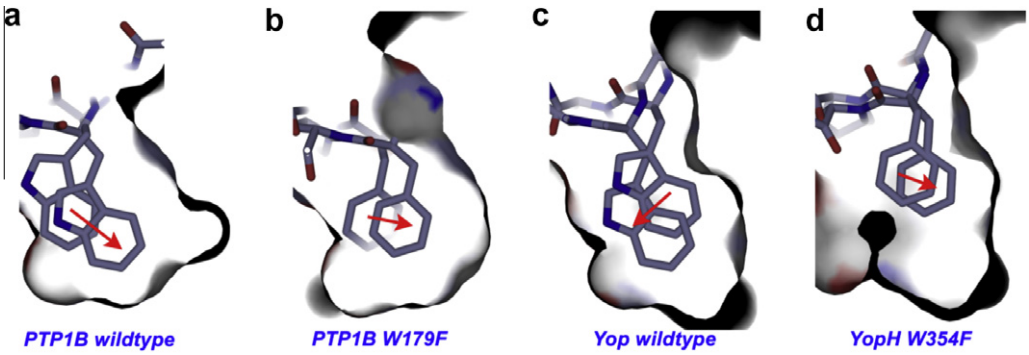

Fig. 4. Comparison between PTP1B and YopH structures. Hydrophobic pocket of the conserved tryptophan in the hinge of the WPD-loop, and orientations of the Trp in the native and Phe in the mutant PTPs in open and closed WPD-loop forms. The arrows indicate the movement direction of the Trp or Phe upon WPD-loop closure. These pictures were made from PTP1B and YopH structures superimposed considering the P-loop region, no rotation was applied between each representation. The hydrophobic pockets for all representations are those for the closed or quasi-open (YopH W354F) WPD-loop conformations. The PDB IDs used to generate each structure were: (a) PTP1B wildtype: 2CM2 (ligand-free form, open WPD-loop) [42], 3I80 (VO_4 bound, closed WPD-loop) [28]; (b) PTP1B W179F: 3QKP (ligand-free form, open WPD-loop), 3QKQ (VO_4 bound, closed WPD-loop); (c) YopH wildtype: 1YPT (ligand-free form, open WPD-loop) [19], 2I42 (VO_4 bound, closed WPD-loop); (d) YopH W354F: 3F99 (ligand-free form, quasi-open WPD-loop), 3F9A (WO_4 bound, quasi-open WPD-loop) [24].

steric clashes upon full loop closure. In contrast, in the YopH wildtype the Trp side chain slides in a direction *opposite* to WPD loop movement. We have previously proposed that the locked quasi-open conformation in the W354F mutant results from steric clashes that would arise between the Phe side chain and important residues (e.g. Pro355 and Thr358) in a fully closed-loop conformation. In fact, the position of Phe354 in the quasi-open loop of W354F YopH closely matches that of Trp354 in the open state of the wildtype enzyme, and shows little difference between the structures of the ligand-free and bound states of YopH W354F [24].

The significantly different responses to the conservative Trp to Phe mutation in YopH compared to PTP1B most likely can be attributed to the opposite direction of motion of this residue's side chain during loop closure. In order to accommodate the new position of the Trp/Phe side chain, other side chains at the pocket (*i.e.* Phe191 and Phe 269) undergo movement in PTP1B upon WPD-loop closure. This is not observed in YopH, and the relatively tight Trp pocket in this enzyme is less suitable for the movement of the Phe side chain. This implies that the Trp/Phe pocket in PTP1B exhibits more plasticity than the corresponding pocket in YopH.

It is likely that the Trp repositioning upon WPD-loop closure participates in control of dynamic events and catalysis in PTPs. Although referred to as the WPD-loop, this flexible region in PTPs consists of a larger segment of approximately 10–12 amino acids. The majority of vertebrate PTPs present two highly conserved proline residues in this loop [41]. On one side of the WPD-loop, the Pro180 (residue numbering for PTP1B) is essential for maintenance of the loop secondary structure, while at the other side the Pro185 forms the upper lid of the Trp pocket and it is involved in the Trp/Phe repositioning. It is interesting to observe that the second highly conserved Pro in this position of human PTPs is not a consensus for bacterial PTPs (a sequence alignment of this region is shown in Fig. S4 of Supporting information). The corresponding position of Pro185 in PTP1B is occupied by Val360 in YopH. In addition to the interplay between side chains of Pro185 and Trp179, the NH indole moiety of the Trp side chain has polar interactions with the main chain carbonyl group of Gly183 in PTP1B; the same interaction is observed with the corresponding residue Thr358 in YopH. The Gly183 is conserved in several vertebrate PTPs, [41] and the Thr358 is found only in bacterial PTPs. Although this Thr is not conserved among bacterial PTPs, it is surely an important residue in YopH. The hydroxyl moiety of Thr358 hydrogen bonds to the carbonyl moiety of Pro355 at the other side of the WPD-loop. This interaction, along with a hydrogen bond between the Pro355 carbonyl and Thr358 amide groups, is probably important for stability of the WPD-loop in the closed position.

The importance of an aromatic hydrophobic side chain in the Trp179 position is shown by the significantly reduced k_{cat} of the W179A mutant, which is 325-fold slower than the native enzyme at pH 5.5. YopH also shows a strong response to the corresponding mutation; the W354A mutant is 476-fold slower than native YopH under similar conditions [25]. The similar k_{cat} values between pH 5.5 and 6.5 [25] and large isotope effects in the leaving group of *p*NPP [27] indicate the loss of general acid catalysis in W354A YopH. The W179A mutation in PTP1B causes similar effects on its pH dependency (Table 2), consistent with an impaired general acid catalysis. Catalysis was too slow to permit measurement of kinetic isotope effects with this mutant.

Conclusions

Although WPD-loop movement is a shared feature of catalysis in the PTP family, the Trp to Phe mutation in the conserved WPD-loop has distinctly different results in PTP1B compared with YopH. The Trp to Phe mutation in the WPD loop of YopH locks the loop in a quasi-open position, compromising general acid catalysis; in contrast, PTP1B functions only slightly less efficiently with this mutation and general acid catalysis is unaffected. Crystal structures reveal that in YopH the indole side chain of this residue moves in a direction opposite to WPD loop movement, while in PTP1B the indole and loop move in the same direction. The former case results in steric clashes that cause the loop of the Phe mutant to assume a static position that does not respond to oxyanion binding.

These results show that some molecular details of loop movement are different in YopH and PTP1B. Structural analysis shows that this difference arises from the opposite direction of movement of the indole side chain as the WPD-loop oscillates between the open and closed positions in the two enzymes. Other differences in neighboring residues in eukaryotic and bacterial sources that form the hydrophobic pocket in which the indole moiety moves also account for differences in the mechanical working of this flexible loop in the PTP family. Presumably, such variations exist in other members of the PTP family as well, and may contribute to variations in catalytic rates. A more complete understanding of the causes underlying the apparent dynamical differences in the

human and the bacterial enzymes may come from solution NMR studies that are underway.

It will be an interesting area of future study to address the extent to which loop movement correlates with catalytic rates in PTPs and whether or not this might explain the variations in catalytic efficiency within this enzyme family.

Acknowledgments

We thank Nick Tonks for providing the plasmid encoding native PTP1B. ACH expresses thanks to John Denu, in whose laboratory some of the initial experiments on this project were carried out during a sabbatical. We are also grateful to CAPES (Brazil) for a Fellowship to T.A.S. Brandão. This research was supported by a Grant from the National Institutes of Health (GM47297).

Appendix A. Supplementary data

Supplementary data associated with this article can be found, in the online version, at http://dx.doi.org/10.1016/j.abb.2012.06.002.

References

[1] T. Hunter, Cell 80 (1995) 225–236.
[2] M.D. Jackson, J.M. Denu, Chemical Reviews 101 (2001) 2313–2340.
[3] Z.-Y. Zhang, Critical Reviews in Biochemistry and Molecular Biology 33 (1998) 1–52.
[4] A. Alonso, J. Sasin, N. Bottini, I. Friedberg, I. Friedberg, A. Osterman, A. Godzik, T. Hunter, J. Dixon, T. Mustelin, Cell 117 (2004) 699–711.
[5] R.R. Brubaker, Clinical Microbiology Reviews 4 (1991) 309–324.
[6] Z.Y. Zhang, J.C. Clemens, H.L. Schubert, J.A. Stuckey, M.W.F. Fischer, D.M. Hume, M.A. Saper, J.E. Dixon, Journal of Biological Chemistry 267 (1992) 23759–23766.
[7] Z.Y. Zhang, A.M. Thiemesefler, D. Maclean, D.J. Mcnamara, E.M. Dobrusin, T.K. Sawyer, J.E. Dixon, Proceedings of the National Academy of Sciences of the United States of America 90 (1993) 4446–4450.
[8] C. Lad, N.H. Williams, R. Wolfenden, Proceedings of the National Academy of Sciences of the United States of America 100 (2003) 5607–5610.
[9] T. Hunter, Cell 100 (2000) 113–127.
[10] S. Zhang, Z.Y. Zhang, Drug Discovery Today 12 (2007) 373–381.
[11] T.O. Johnson, J. Ermolieff, M.R. Jirousek, Nature Reviews Drug Discovery 1 (2002) 696–709.
[12] F.G. Haj, B. Markova, L.D. Klaman, F.D. Bohmer, B.G. Neel, Journal of Biological Chemistry 278 (2003) 739–744.
[13] Z.Y. Zhang, Annual Review of Pharmacology and Toxicology 42 (2002) 209–234.
[14] A. Ostman, C. Hellberg, F.D. Bohmer, Nature Reviews Cancer 6 (2006) 307–320.
[15] A.K. Pedersen, X.L. Guo, K.B. Moller, G.H. Peters, H.S. Andersen, J.S. Kastrup, S.B. Mortensen, L.F. Iversen, Z.Y. Zhang, N.P.H. Moller, Biochemical Journal 378 (2004) 421–433.
[16] Z.Y. Zhang, Current Topics in Cellular Regulation 35 (1997) 21–68.
[17] Z.Y. Zhang, Y.A. Wang, J.E. Dixon, Proceedings of the National Academy of Sciences of the United States of America 91 (1994) 1624–1627.
[18] D. Barford, A.J. Flint, N.K. Tonks, Faseb Journal 8 (1994) A1322.
[19] J.A. Stuckey, H.L. Schubert, E.B. Fauman, Z.Y. Zhang, J.E. Dixon, M.A. Saper, Nature 370 (1994) 571–575.
[20] E.B. Fauman, C. Yuvaniyama, H.L. Schubert, J.A. Stuckey, M.A. Saper, Journal of Biological Chemistry 271 (1996) 18780–18788.
[21] M.R. Groves, Z.J. Yao, P.P. Roller, T.R. Burke, D. Barford, Biochemistry 37 (1998) 17773–17783.
[22] H.L. Schubert, E.B. Fauman, J.A. Stuckey, J.E. Dixon, M.A. Saper, Protein Science 4 (1995) 1904–1913.
[23] A.C. Hengge, Accounts of Chemical Research 35 (2002) 105–112.
[24] T.A.S. Brandao, H. Robinson, S.J. Johnson, A.C. Hengge, Journal of the American Chemical Society 131 (2009) 778–786.
[25] Y.F. Keng, L. Wu, Z.Y. Zhang, European Journal of Biochemistry 259 (1999) 809–814.
[26] D. Barford, J.C. Keller, A.J. Flint, N.K. Tonks, Journal of Molecular Biology 239 (1994) 726–730.
[27] R.H. Hoff, A.C. Hengge, L. Wu, Y.F. Keng, Z.-Y. Zhang, Biochemistry 39 (2000) 46–54.
[28] T.A.S. Brandao, A.C. Hengge, S.J. Johnson, Journal of Biological Chemistry 285 (2010) 15874–15883.
[29] W.W. Cleland, Enzyme mechanisms from isotope effects, in: A. Kohen, H.-H. Limbach (Eds.), Isotope Effects in Chemistry and Biology, CRC Press, Boca Raton, FL, 2006, pp. 915–930.
[30] A.C. Hengge, G.A. Sowa, L. Wu, Z.-Y. Zhang, Biochemistry 34 (1995) 13982–13987.
[31] Z. Otwinowski, W. Minor, Macromolecular Crystallography, Part A 276 (1997) 307–326.
[32] Rigaku/MSC, CrystalClear: An Integrated Program for the Collection and Processing of Area Detector Data, 2006.
[33] A.J. Mccoy, R.W. Grosse-Kunstleve, P.D. Adams, M.D. Winn, L.C. Storoni, R.J. Read, Journal of Applied Crystallography 40 (2007) 658–674.
[34] S. Bailey, Acta Crystallographica Section D-Biological Crystallography 50 (1994) 760–763.
[35] E. Potterton, P. Briggs, M. Turkenburg, E. Dodson, Acta Crystallographica Section D-Biological Crystallography 59 (2003) 1131–1137.
[36] P.D. Adams, R.W. Grosse-Kunstleve, L.W. Hung, T.R. Ioerger, A.J. McCoy, N.W. Moriarty, R.J. Read, J.C. Sacchettini, N.K. Sauter, T.C. Terwilliger, Acta Crystallographica Section D-Biological Crystallography 58 (2002) 1948–1954.
[37] P. Emsley, K. Cowtan, Acta Crystallographica Section D-Biological Crystallography 60 (2004) 2126–2132.
[38] I.W. Davis, A. Leaver-Fay, V.B. Chen, J.N. Block, G.J. Kapral, X. Wang, L.W. Murray, W.B. Arendall 3rd, J. Snoeyink, J.S. Richardson, D.C. Richardson, Nucleic Acids Research 35 (2007) W375–W383.
[39] W.L. DeLano, The PyMOL Molecular Graphics System, DeLano Scientific LLC, Palo Alto, CA, USA, 2007.
[40] A.C. Hengge, FEBS Letters 501 (2001) 99–102.
[41] J.N. Andersen, O.H. Mortensen, G.H. Peters, P.G. Drake, L.F. Iversen, O.H. Olsen, P.G. Jansen, H.S. Andersen, N.K. Tonks, N.P.H. Moller, Molecular and Cellular Biology 21 (2001) 7117–7136.
[42] P.J. Ala, L. Gonneville, M.C. Hillman, M. Becker-Pasha, M. Wei, B.G. Reid, R. Klabe, E.W. Yue, B. Wayland, B. Douty, P. Polam, Z. Wasserman, M. Bower, A.P. Combs, T.C. Burn, G.F. Hollis, R. Wynn, Journal of Biological Chemistry 281 (2006) 32784–32795.